ISSN: 2277-3754
ISO 9001:2008 Certified
International Journal of Engineering and Innovative Technology (IJEIT)
Volume 4, Issue 7, January 2015

Iterative Refinement and Edge Processing in PDE-based Image Restoration

Hwan Hee Park and Seongjai Kim

Department of Computational and Applied Mathematics, Rice University
6100 Main Street, Houston, TX 77005 USA. Email: hwanheepk@yahoo.com.
Department of Mathematics and Statistics, Mississippi State University
Mississippi State, MS 39762 USA. Email: skim@math.msstate.edu.

Abstract*— *This article studies iterative refinement methods and edge processing techniques for PDE-based image restoration. In order to restore fine structures in the image, iterative refinement procedures suggested by Bregman have been introduced in image restoration. However, the Bregman iterative refinement (BIR) first recovers fine scales of the image and then restores the noise in later iterations; the iterates converge to the observed noisy image so that the iteration must be stopped manually when the quality of the obtained image appears satisfactory. This article investigates an effective refinement procedure called the curvature correction method (CCM) to overcome the drawback of the Bregman iteration. By incorporating the curvature estimated from the previous iterate as a source term, the new model can successfully produce a convergent sequence of images having a better restoration quality than the best result of the Bregman procedure. The article also introduces edge-processing variants of BIR and CCM which update image values only on edges in the second and later iterations. When noise level is high, the edge-processing algorithms have produced better images than their original, global-updating methods. Various numerical examples are given to confirm the claim and to show effectiveness of new refinement methods.

***Index Terms*—** Image restoration, denoising, curvature correction method (CCM), Bregman iterative refinement (BIR), partial differential equation (PDE), edge processing.

I. Introduction

As various image processing tasks require higher reliability and efficiency, mathematical techniques have become important components of image processing. During the last two decades or so, mathematical tools of partial differential equations (PDEs) and functional analysis have been successfully applied for various image processing tasks, particularly for image denoising and restoration [2, 4, 6, 10, 12, 14, 15]. Those PDE-based models have allowed researchers and practitioners not only to introduce new, effective computational procedures but also to improve traditional algorithms in image restoration.

However, these PDE-based models tend to either converge to a piecewise constant image or introduce image blur (undesired dissipation), partially because the models are derived by minimizing a functional of the image gradient. As a consequence, the conventional PDE-based models may lose interesting image fine structures. In order to reduce the artifact, researchers have studied various mathematical and numerical techniques which either incorporate more effective constraint terms and iterative refinement [7, 10, 13] or minimize a functional of second derivatives of the image [5, 9]. These new mathematical models may preserve fine structures better than conventional ones; however, more advanced models and appropriate numerical procedures are yet to be developed.

Iterative refinement procedures have been introduced in image restoration [11, 13], employing an original idea of Bregman [1], in order to recover fine structures in the image. The Bregman iterative procedure tries to produce a sequence of images for the signal adjusted by all of the previous residuals. Thus, it recovers not only fine scales of the image but also the noise and reveals a strong tendency to converge to the observed noisy signal. For this reason the Bregman iterative procedure must be stopped *manually* when the quality of the obtained image appears satisfactory.

This article first introduces a new iterative refinement procedure called the *curvature correction method* (CCM) in order to overcome the drawback of the Bregman iteration. The CCM is a variant of the curvature interpolation method [4], which has been studied as an effective image zooming method. In the CCM, the new iterate is computed with the curvature-related (diffusion) term estimated from the last iterate and incorporated as an extra source. It has been numerically verified that the CCM can successfully produce a convergent sequence of images having a compatible restoration quality with the best result of the Bregman iterative procedure.

The article also investigates edge processing methods for a better restoration quality. In slow-transition regions of the image, the first residual (the difference between the observed image and the first iterate) would contain *little* amount of interesting image components; most of the first residual in smooth regions must come from the noise. Thus, the incorporation of the residual over the whole image domain may de-

ISSN: 2277-3754
ISO 9001:2008 Certified
International Journal of Engineering and Innovative Technology (IJEIT)
Volume 4, Issue 7, January 2015

teriorate later iterates in the slow-transition regions, because new iterates are computed with a large noise component for little of interesting image components. This observation has motivated the authors to study an edge processing method for which the second and later iterations are carried out on edges only. The edge processing strategy is applied for both the Bregman iterative refinement and the CCM and their performances are compared with those of the original (global) iterative refinement methods. This article is an extension of the conference proceedings [3]; here we refine the CCM for image restoration and introduce edge processing methods aforementioned and to be discussed in detail in Section IV.

An outline of the paper is as follows. In the following section, PDE-based image denoising models and the Bregman iterative refinement (BIR) are briefly reviewed. Section III describes the curvature correction method, while the edge processing methods are studied in Section IV along with numerical verification. In Section V, further numerical experiments are presented to show effectiveness of the new algorithms. Section VI concludes our development and experiments. In Appendix A, we present effective finite difference schemes for the approximation of the curvature term.

II. Preliminaries

In this section, we present a brief review of PDE-based image denoising models, followed by the Bregman iterative refinement (BIR).

A. PDE-based denoising models

Given an observed (noisy) image $f : \Omega \to \mathbb{R}$, where Ω is the image domain which is an open subset in $\mathbb{R}^2$, we consider the noise model of the form

$$f = u + g(u)\eta, \tag{1}$$

where u is the desired image and $g(u)\eta$ denotes the noise with η having a zero mean. For example, $g(u) = 1$ for Gaussian noise and $g(u) = \sqrt{u}$ for speckle noise in ultrasound images [8]. Then a common denoising technique is to minimize a functional of gradient:

$$u = \arg\min_u \Big\{ \int_\Omega \rho(|\nabla u|)\, d\mathbf{x} + \frac{\lambda}{2} \int_\Omega \Big(\frac{f-u}{g(u)}\Big)^2 d\mathbf{x} \Big\}, \tag{2}$$

where ρ is an increasing function (often, convex) and $\lambda \geq 0$ denotes the constraint parameter. It is often convenient to transform the minimization problem (2) into a differential equation, called the *Euler-Lagrange equation*, by applying the variational calculus [16]:

$$-\psi(u)\, \nabla \cdot \Big(\rho'(|\nabla u|) \frac{\nabla u}{|\nabla u|} \Big) = \lambda\, (f-u), \tag{3}$$

where

$$\psi(u) = \frac{g(u)^3}{g(u) + (f-u)g'(u)}.$$

For an edge-adaptive image denoising, it is required to hold $\rho'(s)/s \to 0$ as $s \to \infty$. For the speckle noise in ultrasound images, Krissian *et al.* [8] set $g(u) = \sqrt{u}$, which implies $\psi(u) = 2u^2/(f+u) \approx u$; the diffusion term becomes large at largely perturbed pixels (speckles) and therefore the resulting model can suppress (positive) speckles more effectively.

When $\rho(s) = s$ and $g(u) \equiv 1$, the model (3) becomes the total variation (TV) model [15]:

$$\kappa(u) \;=\; \lambda(f-u), \qquad \text{(TV)} \tag{4}$$

where $\kappa(u)$ is the negation of the *mean curvature* defined as

$$\kappa(u) = -\nabla \cdot \Big(\frac{\nabla u}{|\nabla u|} \Big). \tag{5}$$

It is often the case that the constraint parameter λ is set as a constant, as suggested by Rudin-Osher-Fatemi [15]. In order to find the parameter, the authors merely multiplied (4) by $(f-u)$ and averaged the resulting equation over the whole image domain Ω:

$$\lambda = \frac{1}{\sigma^2} \frac{1}{|\Omega|} \int_\Omega (f-u)\, \kappa(u)\, d\mathbf{x}, \tag{6}$$

where σ^2 is the noise variance

$$\sigma^2 = \frac{1}{|\Omega|} \int_\Omega (f-u)^2\, d\mathbf{x}. \tag{7}$$

(In [15], λ was evaluated after applying integration by parts for the right-side of (6), which could avoid approximations of second-derivatives.)

As another example of (3), the Perona-Malik (PM) model [14] can be obtained by setting $\rho(s) = \frac{1}{2}K^2 \ln(1 + s^2/K^2)$, for some $K > 0$, and $\lambda = 0$:

$$-\nabla \cdot (c(|\nabla u|)\, \nabla u) = 0, \qquad \text{(PM)} \tag{8}$$

where $c(s) = \rho'(s)/s = (1 + s^2/K^2)^{-1}$. Note that for the PM model, the function ρ is strictly convex for $s < K$ and strictly concave for $s > K$. (K is a threshold.) Thus the model can enhance image content of large gradient magnitudes such as edges and speckles; however, it will flatten regions of slow transitions.

Most of conventional PDE-based restoration models have shown either to converge to a piecewise constant image or to lose fine structures of the given image. Although these results are important for understanding of the current diffusion-like models, the resultant signals may not be desired in applications where the preservation of both slow transitions and fine structures is important.

The TV model tends to converge to a piecewise constant image. Such a phenomenon is called the *staircasing* effect. In order to suppress it, Marquina and Osher [10] suggested to multiply the stationary TV model by a factor of $|\nabla u|$:

$$|\nabla u|\, \kappa(u) \;=\; \lambda\, |\nabla u|\, (f-u). \qquad \text{(ITV)} \tag{9}$$

Since $|\nabla u|$ vanishes only on flat regions, its steady state is analytically the same as that of the TV model (4). We will call

ISSN: 2277-3754
ISO 9001:2008 Certified
International Journal of Engineering and Innovative Technology (IJEIT)
Volume 4, Issue 7, January 2015

(9) the *improved TV* (ITV) model. Such a non-variational reformulation turns out to reduce the staircasing effect successfully; however, it is yet to be improved for a better preservation of fine structures.

The conventional PDE-based denoising models, including ones presented in this section, can be written in the following general form

$$\mathcal{L}(u) = \mathcal{C}(f-u), \tag{10}$$

where $\mathcal{L}$ is a diffusion (smoothing) operator and $\mathcal{C}$ denotes the constraint parameter.

B. The Bregman iterative refinement

In order to recover fine structures in the image, iterative refinement procedures employing an original idea by Bregman [1] have been introduced in image restoration and image zooming [11, 13]. The Bregman iterative refinement (BIR) applied to the general denoising model (10) reads as follows: if u_1 is the solution of (10)

$$\mathcal{L}(u_1) = \mathcal{C}(f-u_1), \tag{11}$$

we denote the corresponding residual by r_1, i.e.,

$$r_1 = f - u_1.$$

Then we again solve the model with the signal replaced by $f + r_1$; the solution u_2 will satisfy

$$\mathcal{L}(u_2) = \mathcal{C}(f + r_1 - u_2), \tag{12}$$

and the new residual is defined as

$$r_2 = f + r_1 - u_2.$$

In general, the m-th iterate of Bregman iteration, u_m, is computed as the restoration for the signal $f + r_{m-1}$, i.e.,

$$\mathcal{L}(u_m) = \mathcal{C}(f + r_{m-1} - u_m), \quad m \geq 1, \tag{13}$$

where $r_0 = 0$, and the new residual is defined as

$$r_m = f + r_{m-1} - u_m. \tag{14}$$

As for other conventional PDE-based denoising models, each step of the Bregman iteration (13) may be parameterized by an artificial time t for a convenient numerical simulation. That is, u_m can be considered as an evolutionary function and the corresponding evolutionary equation can be obtained by adding $\frac{du_m}{dt}$ on the left side of (13).

$$\frac{du_m}{dt} + \mathcal{L}(u_m) = \mathcal{C}(f + r_{m-1} - u_m). \quad m \geq 1. \tag{15}$$

The explicit temporal discretization of (15) can be formulated as

$$u_m^n = u_m^{n-1} + \Delta t \left[-\mathcal{L}(u_m^{n-1}) + \mathcal{C}(f + r_{m-1} - u_m^{n-1})\right], \tag{16}$$

where $u_m^0 = u_{m-1}$ and Δt denotes the temporal stepsize.

As indicated in [11], the Bregman iterative procedure first recovers fine scales of the image and then recovers the noise to converge to the observed noisy image f. For this reason the Bregman iterative procedure must be stopped *manually* when the quality of the obtained image appears satisfactory. Notice that the residuals r_m in (14) read

$$\begin{aligned} r_m &= (f-u_m) + r_{m-1} \\ &= (f-u_m) + (f-u_{m-1}) + r_{m-2} \\ &= \cdots = \sum_{i=1}^{m} (f-u_i). \end{aligned} \tag{17}$$

Thus the m-th iterate of Bregman iteration, u_m, is computed for the signal

$$f + r_{m-1} = f + \sum_{i=1}^{m-1} (f-u_i), \tag{18}$$

which is the original image f added by differences between each of the previous iterates and f. The additive amendment makes the constraint term accentuated, which in return forces the new iterate u_m become closer to f. One may try to modify the last term in (18), by either normalizing or smoothing, in order to prevent the iterates u_m from converging to the noisy image f. However, every trial has failed to improve image quality.

An research objective in this article is to develop PDE-based, iterative refinement denoising models which can restore images effectively and stop *automatically* satisfying the user-defined stopping criterion.

III. The Curvature Correction Method

As an iterative refinement model for the basic restoration model of the form (10), we suggest the following. Given a noisy image f, set $v_0 = 0$ and find v_m by recursively solving

$$\mathcal{L}(v_m) = \mathcal{C}(f - v_m) + \mathcal{L}(v_{m-1}), \quad m \geq 1. \tag{19}$$

Recall that $\mathcal{L}(v_{m-1})$ is the curvature-related diffusion term estimated from the last iterate v_{m-1}.

The new model deserves the following remarks.

1. Utilizing (13) and (14), the Bregman iterative procedure can be rewritten as

   $$\mathcal{L}(u_m) = \mathcal{C}\, r_m = \mathcal{C}(f-u_m) + \mathcal{C}\, r_{m-1}.$$

   When the problem is solved *exactly* in each iteration, we have $\mathcal{L}(u_m) = \mathcal{C}\, r_m$ for all $m \geq 1$. Thus the last term of the above equation, $\mathcal{C}\, r_{m-1}$, can be replaced by $\mathcal{L}(u_{m-1})$:

   $$\mathcal{L}(u_m) = \mathcal{C}(f-u_m) + \mathcal{L}(u_{m-1}). \tag{20}$$

   Since the first iterates of (13) and (19) are the same each other, i.e., $v_1 = u_1$, it follows from (19) and (20) that $v_m = u_m$ for all $m \geq 1$. In practice, however, it is often the case that each step in (13) is solved *approximately*, employing an iterative linearized solver (inner iteration) as in (16). Thus $\mathcal{L}(u_{m-1})$ differs from $\mathcal{C}\, r_{m-1}$ and therefore v_m is not the same as u_m in general.

ISSN: 2277-3754
ISO 9001:2008 Certified
International Journal of Engineering and Innovative Technology (IJEIT)
Volume 4, Issue 7, January 2015

2. It has been numerically verified that as m grows, the iterates of the new algorithm v_m shows a tendency of gaining the noise from the observed image f, but the tendency is weak enough to be stopped automatically satisfying a user-given stopping criterion. In this article the iterative refinement model in (19) will be called the *curvature correction method* (CCM) for image denoising. Note that the CCM can be considered as a variant of the curvature interpolation method [4] that is developed for image interpolation with different derivation principles. However, they are closely related. The major theme is the incorporation of the curvature-related diffusion term as an extra source.

As for the Bregman iterative refinement, each step of the new denoising model (19) can be parameterized by an artificial time t for a convenient numerical simulation.

$$\frac{dv_m}{dt} + \mathcal{L}(v_m) = \mathcal{C}(f - v_m) + \mathcal{L}(v_{m-1}), \quad m \geq 1. \quad (21)$$

Its equilibrium solution is a smooth, restored image of f with the extra source term $\mathcal{L}(v_{m-1})$ incorporated as a correction term. It has been numerically verified that the extra source term allows the new iterate v_m to restore fine features effectively. The explicit temporal discretization of (21) reads

$$\begin{aligned} v_m^n &= v_m^{n-1} + \Delta t \left[-\mathcal{L}(v_m^{n-1}) \right. \\ &\quad \left. + \mathcal{C}(f - v_m^{n-1}) + \mathcal{L}(v_{m-1}) \right], \end{aligned} \quad (22)$$

where $v_m^0 = v_{m-1}$ and Δt is the temporal stepsize. The algorithm (22) is an inner loop solving for v_m and can be viewed as the Richardson iterative method for (19).

Effective numerical schemes for the approximation of $\mathcal{L}(u)$ is presented in Appendix A.

IV. Edge Processing Methods

When stopped appropriately, iterative refinement methods such as BIR and CCM can improve the image quality, particularly around edges. However, those iterative methods may deteriorate slow-transition regions when the noise level is high. In order to illustrate this and to find a remedy, this section begins with an example.

Figure 1 shows denoising results by BIR, of which the basic model is the ITV (9). The noisy image in Figure 1(a) is obtained by perturbing the original Lena image in Figure 5(h) below by a Gaussian noise of PSNR=20.17. By PSNR, we mean the *peak signal-to-noise ratio* (PSNR); the PSNR of f is defined as

$$\text{PSNR} \equiv 10 \log_{10} \left(\frac{\sum_{ij} 255^2}{\sum_{ij} (g_{ij} - f_{ij})^2} \right) \text{dB},$$

where g denotes the original (desirable) image. As one can see from the figure, BIR fails to improve the image quality in the second iteration. Note that the second iteration incorporates the residual from the first iterate, as an extra component of the constraint term; see (12). The extra component may deteriorate the image content particularly on slow-transition regions, as shown in Figure 1(c).

In order to see the details, we present curve plots in Figure 2, for which the data are obtained from a central part (the 50th to the 200th pixels) of the 64th horizontal line of the original Lena image, the noisy image, u_1, and u_2. The image is restored reasonably well in the first iteration of BIR, although the noisy image involves a high level of noise. The second iteration of BIR has improved the image quality on most of edges. But it has introduced a certain degree of degradation on slow-transition regions; see the curves, for example, on the 70th to 90th pixels and the 130th through 150th pixels. The degradation on slow-transition regions is due to the first residual r_1 incorporated as an extra component in the constraint term.

It is now well-known that most of classical PDE-based denoising models show a tendency to introduce image blur on edges. The image blur on edges can be reduced through iterative refinements. However, slow-transition regions may not need to be updated, because the PDE-based denoising models can restore the image successfully there in a single iteration. This observation has motivated the authors to introduce the following edge processing algorithm, in which the iterative refinement updates image values only on edges in the second and later iterations.

$$\begin{aligned} &\text{(i)} && \text{Solve (11) for } u_1, \\ &&& \quad \mathcal{L}(u_1) = \mathcal{C}(f - u_1); \\ &\text{(ii)} && \text{Detect edges} \\ &&& \quad E = (u_1 > T); \\ &\text{(iii)} && \text{Apply BIR (13) or CCM (19),} \\ &&& \quad \text{only on } E, \text{ for } m \geq 2; \end{aligned} \quad (23)$$

Here T denotes a threshold; as for the default threshold for a Matlab command `edge`, one may set

$$T = 2 \cdot \text{mean}(u_1). \quad (24)$$

In this article, the edge processing algorithm (23) will be called BIR$_E$ or CCM$_E$ depending on the use of BIR or CCM for the second and later iterations.

Figure 3 exhibits the second iterates of BIR$_E$ and CCM$_E$, along with u_1, which are restored from the same noisy Lena image in Figure 1(a). Both of the second iterates show a better image quality than the first iterate, in visual content and PSNR values as well, although they are updated only once on edges. They look sharper than the first iterate, while CCM$_E$ performs better than BIR$_E$.

In order to see the details, we show curve plots in Figure 4, where the data are obtained again from the 64th horizontal line of the original Lena image g, the first iterate u_1, and second iterates of BIR$_E$ and CCM$_E$. The second iterates are updated only on edges; for example, see the curves around the 70th, the 170th, and the 190th pixels. BIR$_E$ and CCM$_E$ have improved the image similarly in the vicinity of

ISSN: 2277-3754
ISO 9001:2008 Certified
International Journal of Engineering and Innovative Technology (IJEIT)
Volume 4, Issue 7, January 2015

(a) (b) (c)

Fig. 1. Lena in 256×256 pixels: (a) A noisy image, (b) the first iterate of BIR, u_1 (PSNR=28.61), and (c) the second iterate of BIR, u_2 (PSNR=27.07). The noisy image is obtained by perturbing Figure 5(h) below by a Gaussian noise of PSNR=20.17.

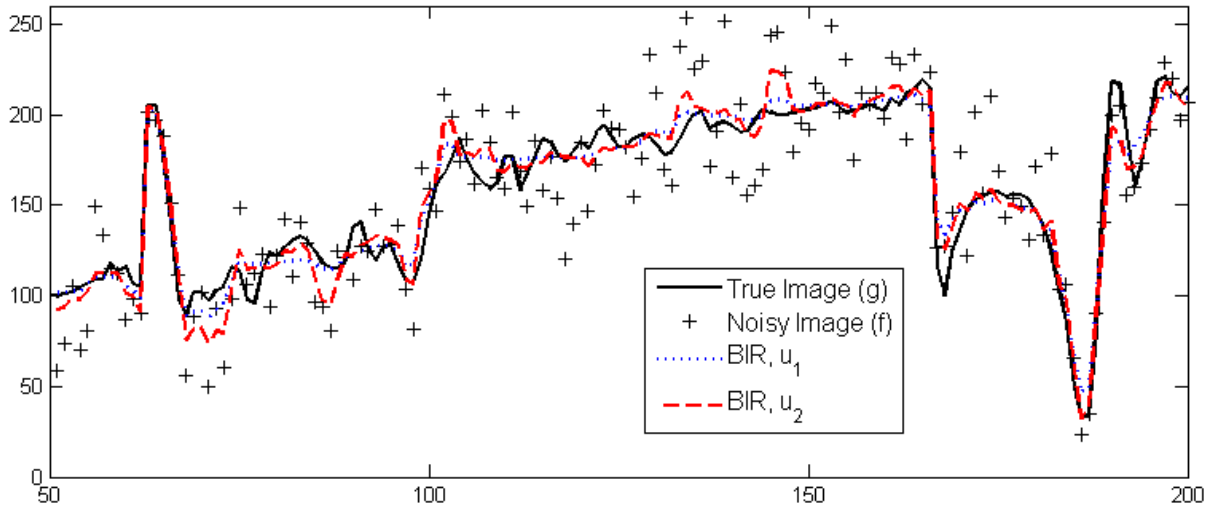

Fig. 2. Curve plots: The data are obtained from the 64th horizontal line of the original Lena image g, the noisy image f, u_1, and u_2. The horizontal axis is indexed for the 50th to the 200th pixels, while the vertical axis is for the image values ranging between 0 and 255.

(a) (b) (c)

Fig. 3. Lena: (a) the first iterate, u_1 (PSNR=28.61), (b) the second iterate of BIR_E (PSNR=28.62), and (c) the second iterate of CCM_E (PSNR=28.94).

ISSN: 2277-3754
ISO 9001:2008 Certified
International Journal of Engineering and Innovative Technology (IJEIT)
Volume 4, Issue 7, January 2015

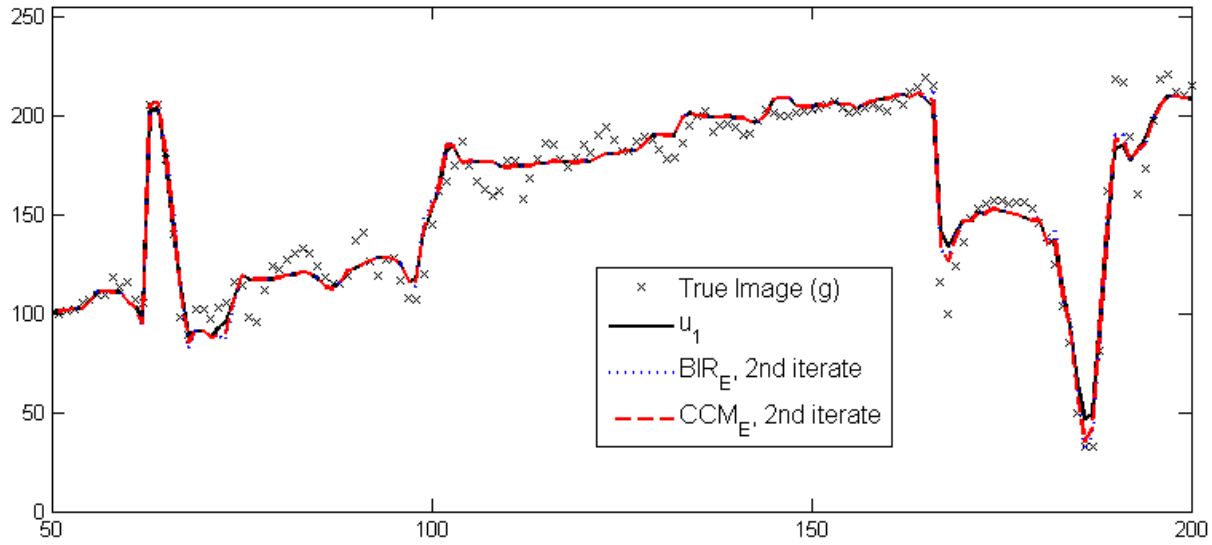

Fig. 4. Curve plots: The data are obtained from the 64th horizontal line of the original Lena image, the first iterate u_1, and second iterates of BIR_E and CCM_E.

the 190th pixel, while CCM_E has outperformed BIR_E near the 170th pixel. In a neighborhood of the 70th pixel, both BIR_E and CCM_E have deteriorated the image due to a heavy noise there; however, BIR_E is more sensitive to the noise to make the restored image worse than CCM_E. It has been numerically verified that when images carry high levels of noise, majority of them prefer to be restored by CCM instead of BIR, whether the iterative refinement algorithms are applied globally over the whole domain or on edges only.

More examples are given in the following section to verify the claim.

V. Further Numerical Experiments

In order to further investigate properties of the BIR and CCM and their variants for edge processing, sample images are downloaded from public domains, as shown in Figure 5. For all examples to be presented in this section, we choose the ITV (9) for the basic denoising model, with λ being selected the best heuristically. For the solutions of inner loops, we set $\Delta t = 0.2$ for (16) and (22). The inner loops are solved roughly and stopped when either the maximum difference between consecutive iterates is bounded by 3.0 or the number of iterations becomes 50.

In Tables 1, we present a PSNR analysis. Each of the 10 sample images in Figure 5 is first deteriorated by a Gaussian noise. The four algorithms (BIR, CCM, BIR_E, and CCM_E) are applied to obtain a sequence of restored images, beginning from the noisy image (f). Then, PSNR values are computed to measure the differences between the restored images and the original image of no noise. The largest PSNR values are reported in the table; the numbers in parentheses denote the number of outer iterations for the method to reach at the best PSNR, for the noise image of the specified noise level. When the noise level is low (as in the top half of the table), the best restoration can be obtained by either BIR or CCM for all images except the Disk image. Note that BIR_E and CCM_E update the restoration only on edges in the second and later iterations. Such edge processing improves image quality, but not better than their global versions (BIR and CCM) when the noise level is low.

On the other hand, when the noise level is high (as in the bottom half of the table), the best restoration has been achieved by one of the edge processing methods for all images. As one can see from the table, BIR could improve the image quality in the second iteration for three images (Airplane, Car, and Disk). For other images, BIR failed to refine in the second and later iterations and produced a sequence of images rapidly converging to the noise image. CCM has performed better than BIR for more images, for high levels of noise. It has been observed (see Table 2 below) that CCM is much less sensitive to the noise than BIR and returns little of the noise back to its iterates. This implies that CCM can restore images *satisfactorily* and in a *converging* sequence. The edge processing variant of CCM, CCM_E, could enhance image quality for all heavily noised images except the Dog image, performing better than other methods for most images. However, the major merit of CCM and CCM_E is not on higher PSNR values they can get, but on their convergence behavior. CCM and CCM_E converge to a desirable image other than the noisy image.

Note that when the noise level is high, the edge-processing variants can restore images equal to or better than their global-processing methods. This implies that iterative refinement methods can barely improve the image quality for

ISSN: 2277-3754
ISO 9001:2008 Certified
International Journal of Engineering and Innovative Technology (IJEIT)
Volume 4, Issue 7, January 2015

Table 1. Best PSNR values. The numbers in parentheses denote the number of outer iterations for the method to reach at the best PSNR.

	f	BIR	CCM	BIR_E	CCM_E
Airplane	26.34	**31.36**(3)	31.20(3)	30.34(4)	30.26(4)
Balloons	26.26	33.87(2)	**33.97**(2)	33.57(2)	33.60(2)
Car	25.98	29.87(3)	**30.00**(4)	29.22(5)	29.23(5)
Disk	25.99	40.03(3)	39.90(3)	40.26(3)	**40.27**(3)
Dog	26.09	**31.35**(2)	31.32(2)	31.32(2)	31.29(2)
Elaine	26.32	31.11(2)	**31.18**(2)	30.97(2)	30.97(2)
Fire	26.57	32.52(2)	**32.54**(3)	31.80(3)	31.87(3)
Lena	26.38	**32.28**(2)	32.14(3)	31.39(3)	31.35(3)
Stones	25.99	**31.82**(2)	31.72(2)	31.53(2)	31.48(2)
Swan	25.95	**32.22**(2)	32.17(2)	32.05(2)	32.01(2)
Airplane	21.46	28.08(2)	28.09(3)	**28.18**(2)	28.17(4)
Balloons	22.12	31.51(1)	31.59(2)	31.58(3)	**31.63**(3)
Car	22.34	27.69(2)	27.60(3)	27.70(3)	**27.81**(4)
Disk	21.40	34.76(2)	34.61(1)	**35.52**(2)	35.39(2)
Dog	21.09	29.44(1)	29.44(1)	29.44(1)	29.44(1)
Elaine	21.42	29.09(1)	29.17(2)	29.09(1)	**29.19**(3)
Fire	21.72	29.72(1)	29.94(2)	29.73(2)	**29.96**(4)
Lena	21.90	29.31(1)	29.63(2)	29.32(2)	**29.66**(3)
Stones	22.51	29.74(1)	30.05(2)	29.82(2)	**30.07**(3)
Swan	21.31	30.00(1)	30.00(1)	30.00(1)	**30.02**(2)

heavily noised images in slow-transition zones, as we already analyzed in the previous section. It also should be noticed that CCM is comparable with BIR, whether the noise level is high or not.

Table 2 includes a convergence analysis for the four methods to run five iterations. The Lena image is exemplified for the analysis and PSNR values are recorded in each iteration. Note that the first iterate is the same for all of four methods. For the Lena image, BIR reaches at its largest PSNR value in one or two iterations and runs a sharp downhill. Although PSNR is not always a good indicator for quality control, it is clear to see that each iteration of BIR introduces a large change to its iterate. BIR recovers not only fine scales of the image but also the noise and reveals a strong tendency to converge to the observed noisy signal, as already seen in Figure 1. For this reason, in realistic situations in which the true image is unknown, the Bregman iterative procedure must be stopped *manually* when the quality of the obtained image appears satisfactory. BIR_E shows a similar pattern on the PSNR evolution as BIR. Only the difference is that BIR_E changes the PSNR by smaller amounts (due to its application to edges only). On the other hand, CCM and CCM_E have produced a sequence of images whose PSNR values linger after reaching at the maximum. The algorithms have converged in 4 and 3 iterations respectively for the low and the high levels of noise, when the stopping criterion is set as

$$\|v_m - v_{m-1}\|_\infty < 2.$$

Table 2. Convergence analysis: the PSNR values are obtained for the first five iterations when the methods are applied for the restoration of the Lena image.

	f	1	2	3	4	5
BIR	26.38	30.62	**32.28**	31.48	30.19	29.26
CCM	26.38	30.62	31.95	**32.14**	32.13	–
BIR_E	26.38	30.62	31.36	**31.39**	31.26	31.09
CCM_E	26.38	30.62	31.30	**31.35**	31.34	–
BIR	21.90	**29.31**	28.76	27.06	25.97	25.23
CCM	21.90	29.31	**29.63**	29.62	–	–
BIR_E	21.90	29.31	**29.32**	28.99	28.65	28.36
CCM_E	21.90	29.31	29.65	**29.66**	–	–

That is, the maximum norm of the difference between consecutive iterates is less than 2. (One may choose a smaller tolerance. However, it make the algorithms run longer without producing observable differences in image quality.) With the above stopping criterion, CCM and CCM_E have converged in 3-7 iterations for all test images shown in Table 1; the last iterates differ barely from the images of best PSNR values.

Figure 6 contains restored images by the four methods that show the best PSNR. When the noise level is low (the top row of the figure), BIR produces the best image in its second iteration as shown in Figure 6(a). The result of BIR is better than other images in Figures 6(b)–(d), although it is not easy to see differences from visual inspection. When the noise

ISSN: 2277-3754
ISO 9001:2008 Certified
International Journal of Engineering and Innovative Technology (IJEIT)
Volume 4, Issue 7, January 2015

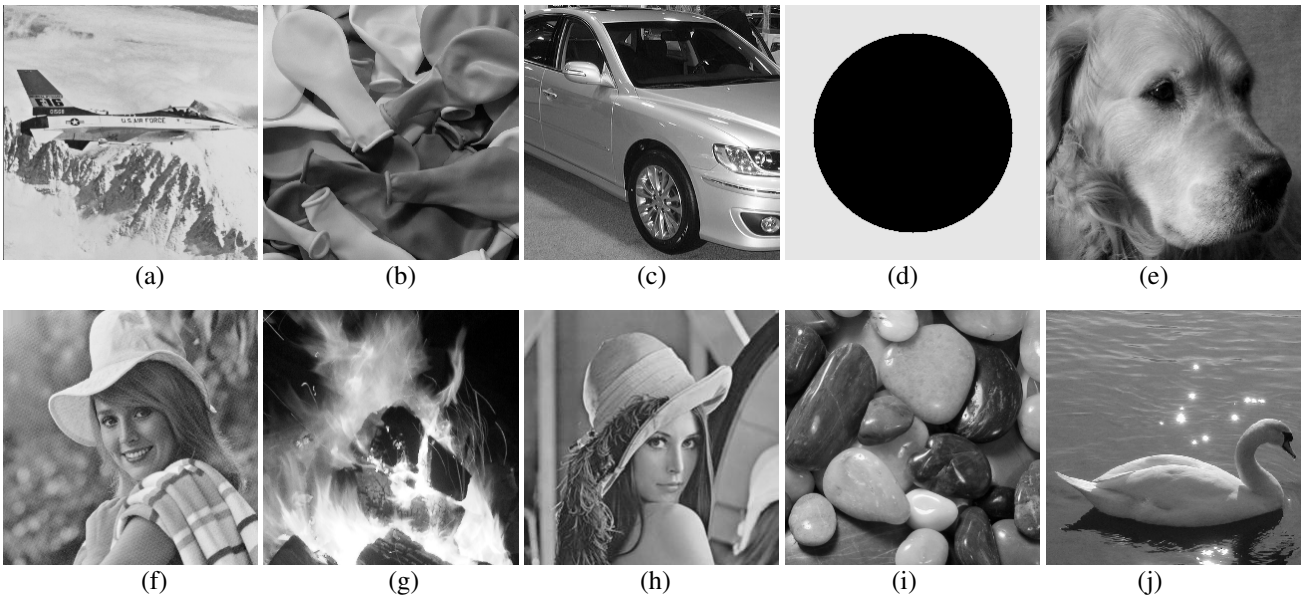

Fig. 5. Sample images: (a) Airplane, (b) Balloons, (c) Car, (d) Disk, (e) Dog, (f) Elaine, (g) Fire, (h) Lena, (i) Stones, and (j) Swan. All are gray-scaled and of 256×256 pixels; they are downloaded from public domains.

level is high, BIR failed to upgrade the image in the second and later iterations. Thus, Figure 6(e) shows its first iterate (u_1), which is the same as the solution of the ITV model (9). CCM has improved the image in its second iteration as shown in Figure 6(f), which looks sharper than u_1. The result of BIR$_E$ in Figure 6(g) is slightly changed from u_1; however, it involves observable noise on edges as seen on the nasal bridge, for example. The last image of the figure is obtained by two edge-processing iterations by CCM$_E$ starting from u_1. It is the same in slow-transition regions as u_1; it looks sharper overall, due to the improvement on edges. The visual inspection is consistent with the PSNR analysis presented in Table 1.

VI. Conclusions

This article studies iterative refinement methods and introduces edge processing techniques for PDE-based image restoration models, in order to restore fine structures in the image. We have observed that the Bregman iterative refinement (BIR) first recovers fine scales of the image and then restores the noise for the iterates to converge to the observed noisy image; it must be stopped *manually* when the quality of the obtained image appears satisfactory. To overcome the drawback of the BIR, we have investigated an effective refinement procedure called the curvature correction method (CCM). By incorporating the curvature estimated from the last iterate as a source term, the new model has been able to successfully produce a convergent sequence of images having a better restoration quality than the best result of the Bregman procedure. Then the article has introduced edge-processing variants of BIR and CCM which update image values only on edges in the second and later iterations. It has been numerically verified that when noise level is high, the edge-processing variants have produced better images than their original, global-updating methods.

A. Finite Difference Schemes for the Diffusion Term

Here we present effective finite difference schemes for the approximation of $\mathcal{L}(u)$. For simplicity, we exemplify the gradient-weighted curvature as in the ITV:

$$\mathcal{L}(u) = -|\nabla u| \, \nabla \cdot \Big(\frac{\nabla u}{|\nabla u|} \Big). \tag{25}$$

First, we rewrite $\mathcal{L}(u)$ by

$$\mathcal{L}(u) = -|\nabla u|_1 \Big(\frac{u_x}{|\nabla u|} \Big)_x - |\nabla u|_2 \Big(\frac{u_y}{|\nabla u|} \Big)_y, \tag{26}$$

where both $|\nabla u|_1$ and $|\nabla u|_2$ are the same as $|\nabla u|$; they will be approximated in a different way. The following numerical schemes are of second-order accuracy; however, they are specifically designed in order for the resulting algebraic system to have the same positive entry on its main diagonal and to become a weighted averaging in its Jacobi iteration.

For each (i, j)-th pixel, we first compute the second-order finite difference approximations of $|\nabla u|$ at $\mathbf{x}_{i-1/2,j}$ (W), $\mathbf{x}_{i+1/2,j}$ (E), $\mathbf{x}_{i,j-1/2}$ (S), and $\mathbf{x}_{i,j+1/2}$ (N):

ISSN: 2277-3754
ISO 9001:2008 Certified
International Journal of Engineering and Innovative Technology (IJEIT)
Volume 4, Issue 7, January 2015

Fig. 6. Lena: Restored images of the best PSNR by (a) BIR, (b) CCM, (c) BIR$_E$, and (d) CCM$_E$, when the noise PSNR=26.28; (e) BIR (u_1), (f) CCM, (g) BIR$_E$, and (h) CCM$_E$, when the noise PSNR=21.90.

$$\begin{aligned} d_{ij,W} &= [(u_{i,j}-u_{i-1,j})^2+(u_{i-1,j+1}+u_{i,j+1} \\ &\quad -u_{i-1,j-1}-u_{i,j-1})^2/16+\varepsilon^2]^{1/2}, \\ d_{ij,E} &= d_{i+1,j,W}, \\ d_{ij,S} &= [(u_{i,j}-u_{i,j-1})^2+(u_{i+1,j}+u_{i+1,j-1} \\ &\quad -u_{i-1,j}-u_{i-1,j-1})^2/16+\varepsilon^2]^{1/2}, \\ d_{ij,N} &= d_{i,j+1,S}, \end{aligned} \tag{27}$$

where $\varepsilon > 0$ is the regularization parameter introduced to prevent the differences from approaching zero. Then, the directional curvature terms at the pixel point $\mathbf{x}_{ij}$ can be approximated as

$$\begin{aligned} \Big(\frac{u_x}{|\nabla u|}\Big)_x(\mathbf{x}_{ij}) &\approx \frac{1}{d_{ij,W}}u_{i-1,j}-\Big(\frac{1}{d_{ij,W}}+\frac{1}{d_{ij,E}}\Big)u_{ij} \\ &\quad +\frac{1}{d_{ij,E}}u_{i+1,j}, \\ \Big(\frac{u_y}{|\nabla u|}\Big)_y(\mathbf{x}_{ij}) &\approx \frac{1}{d_{ij,S}}u_{i,j-1}-\Big(\frac{1}{d_{ij,S}}+\frac{1}{d_{ij,N}}\Big)u_{ij} \\ &\quad +\frac{1}{d_{ij,N}}u_{i,j+1}. \end{aligned} \tag{28}$$

Now, we discretize the gradient magnitudes as follows.

$$\begin{aligned} |\nabla u|_1(\mathbf{x}_{ij}) &\approx \Big[\frac{1}{2}\Big(\frac{1}{d_{ij,W}}+\frac{1}{d_{ij,E}}\Big)\Big]^{-1}=\frac{2\,d_{ij,W}\cdot d_{ij,E}}{d_{ij,W}+d_{ij,E}}, \\ |\nabla u|_2(\mathbf{x}_{ij}) &\approx \Big[\frac{1}{2}\Big(\frac{1}{d_{ij,S}}+\frac{1}{d_{ij,N}}\Big)\Big]^{-1}=\frac{2\,d_{ij,S}\cdot d_{ij,N}}{d_{ij,S}+d_{ij,N}}, \end{aligned} \tag{29}$$

where the right-hand sides are harmonic averages of finite difference approximations of $|\nabla u|$ in x- and y-coordinate directions, respectively. Then, it follows from (26), (28), and (29) that

$$\begin{aligned} \mathcal{L}(u)(\mathbf{x}_{ij}) &\approx 4u_{ij}-a_{ij,W}\,u_{i-1,j}-a_{ij,E}\,u_{i+1,j} \\ &\quad -a_{ij,S}\,u_{i,j-1}-a_{ij,N}\,u_{i,j+1}, \end{aligned} \tag{30}$$

where

$$\begin{aligned} a_{ij,W} &= \frac{2\,d_{ij,E}}{d_{ij,W}+d_{ij,E}}, \quad a_{ij,E}=\frac{2\,d_{ij,W}}{d_{ij,W}+d_{ij,E}}, \\ a_{ij,S} &= \frac{2\,d_{ij,N}}{d_{ij,S}+d_{ij,N}}, \quad a_{ij,N}=\frac{2\,d_{ij,S}}{d_{ij,S}+d_{ij,N}}. \end{aligned}$$

Here $a_{ij,W}+a_{ij,E}+a_{ij,S}+a_{ij,N}=4$. Thus the gradient-weighted curvature can be expressed algebraically as

$$L = A\mathbf{u}, \tag{31}$$

where $\mathbf{u}$ represents the given image, L denotes the second-order finite difference approximation of the gradient-weighted curvature, and A is the coefficient matrix, of which the nonzero elements corresponding to the 5-point stencil centered at $\mathbf{x}_{ij}$ are

$$[A]_{ij} = (-a_{ij,S},\, -a_{ij,W},\, 4,\, -a_{ij,E},\, -a_{ij,N}). \tag{32}$$

Remarks:

1. For the evaluation of $\mathcal{L}(u)$ on the boundary, one has to apply a boundary condition. The boundary condition may affect the final outcome near the boundary. In

ISSN: 2277-3754
ISO 9001:2008 Certified
International Journal of Engineering and Innovative Technology (IJEIT)
Volume 4, Issue 7, January 2015

this article, we employ the no-flux boundary condition: $\nabla u \cdot \mathbf{n} = 0$, where $\mathbf{n}$ denotes the unit outward normal defined on the image boundary.

2. The matrix A in (31) having nonzero elements as in (32) is a diffusion matrix, of which the Jacobi matrix is a weighted averaging operator. Consider a matrix splitting $A = D - N$, where D and $-N$ denote the diagonal and the off-diagonal matrices of A, respectively. Then the Jacobi matrix is $D^{-1}N$, whose elements corresponding to the 5-point stencil centered at $\mathbf{x}_{ij}$ are

$$[D^{-1}N]_{ij} = \Big(\frac{a_{ij,S}}{4}, \frac{a_{ij,W}}{4}, 0, \frac{a_{ij,E}}{4}, \frac{a_{ij,N}}{4}\Big).$$

Since $a_{ij,W} + a_{ij,E} + a_{ij,S} + a_{ij,N} = 4$, the Jacobi matrix is an averaging operator incorporating four neighboring values.

ACKNOWLEDGMENT

S. Kim's work is supported in part by NSF grant DMS-1228337. H. H. Park is a college student, freshman, attending Rice University, Houston, TX, USA. S. Kim deeply appreciates Ms. Park's efforts and contribution to this image processing research.

REFERENCES

[1] L. Bregman, "The relaxation method of finding the common point of convex sets and its application to the solution of problems in convex programming," *USSR Computational Mathematics and Mathematical Physics*, vol. 7, no. 3, pp. 200–217, 1967.

[2] T. Chan, S. Osher, and J. Shen, "The digital TV filter and nonlinear denoising," *IEEE Trans. Image Process.*, vol. 10, no. 2, pp. 231–241, 2001.

[3] A. Gautam, J. Kim, D. Kwak, and S. Kim, "Iterative refinement by smooth curvature correction for PDE-based image restoration," in *Proceedings of The 2013 International Conference on Image Processing, Computer Vision, and Pattern Recognition*, 2013, pp. 518–523.

[4] H. Kim, Y. Cha, and S. Kim, "Curvature interpolation method for image zooming," *IEEE Trans. Image Process.*, vol. 20, no. 7, pp. 1895–1903, 2011.

[5] S. Kim, "Image denoising by fourth-order PDEs," in *Proceedings of the Eighth IASTED International Conference on Signal and Image Processing*, 2006, pp. 249–254.

[6] ——, "PDE-based image restoration: A hybrid model and color image denoising," *IEEE Trans. Image Processing*, vol. 15, no. 5, pp. 1163–1170, 2006.

[7] S. Kim and H. Lim, "A non-convex diffusion model for simultaneous image denoising and edge enhancement," *Electronic Journal of Differential Equations, Conference Special Issue*, vol. 15, pp. 175–192, 2007.

[8] K. Krissian, R. Kikinis, C. F. Westin, and K. Vosburgh, "Speckle-constrained filtering of ultrasound images," in *IEEE Computer Vision and Pattern Recognition or CVPR*, 2005, pp. II: 547–552.

[9] M. Lysaker, A. Lundervold, and X.-C. Tai, "Noise removal using fourth-order partial differential equation with applications to medical magnetic resonance images in space and time," *IEEE Trans. Image Process.*, vol. 12, no. 12, pp. 1579–1590, 2003.

[10] A. Marquina and S. Osher, "Explicit algorithms for a new time dependent model based on level set motion for nonlinear deblurring and noise removal," *SIAM J. Sci. Comput.*, vol. 22, pp. 387–405, 2000.

[11] ——, "Image super-resolution by TV-regularization and Bregman iteration," *J. Sci. Comput.*, vol. 37, pp. 367–382, 2008.

[12] M. Nitzberg and T. Shiota, "Nonlinear image filtering with edge and corner enhancement," *IEEE Trans. on Pattern Anal. Mach. Intell.*, vol. 14, pp. 826–833, 1992.

[13] S. Osher, M. Burger, D. Goldfarb, J. Xu, and W. Yin, "An iterative regularization method for total variation-based image restoration," *Multiscale Model. Simul.*, vol. 4, no. 2, pp. 460–489, 2005.

[14] P. Perona and J. Malik, "Scale-space and edge detection using anisotropic diffusion," *IEEE Trans. on Pattern Anal. Mach. Intell.*, vol. 12, pp. 629–639, 1990.

[15] L. Rudin, S. Osher, and E. Fatemi, "Nonlinear total variation based noise removal algorithms," *Physica D*, vol. 60, pp. 259–268, 1992.

[16] R. Weinstock, *Calculus of Variations*. New York: Dover Pubilcations, Inc., 1974.

Ms. Hwan Hee Park is a freshman attending Rice University, Houston, TX, USA. She is interested in applied mathematics and its applications to real world ptoblems.

Dr. Seongjai Kim received his Ph.D. from Mathematics, Purdue University, in 1995. He is currently a professor of Mathematics and Statistics at Mississippi State University. Dr. Kim's research areas include image processing, computational seismology, and computational fluid dynamics. He has published a book and approximately 75 articles.